ICAS 2021 SHANG HAI
International Council of the Aeronautical Sciences
32nd Congress of the International Council of the Aeronautical Sciences
September 6-10, 2021 Pudong Shangri-La, Shanghai, China

AEROSERVOELASTIC OPTIMIZATION OF A HIGH ASPECT TRANSPORT WING WITH MORPHING TRAILING EDGE

Zhenkai Zhang[1,2], Yongjian Yang[1], Sergio Ricci[2], Alessandro De Gaspari [2], Chen Song[1,3] & Chao Yang[1]

[1]School of Aeronautic Science and Engineering, Beihang University, Beijing 100191, China.
[2]Department of Aerospace Science and Technology, Politecnico di Milano, 20156 Milano, Italy.
[3]Institute of Unmanned System, Beihang University, Beijing 100191, China.

Abstract

The flutter characteristics of a high aspect ratio wing with morphing trailing edges are analyzed based on the assumption mode method and Double-Lattice Method. The unsteady aerodynamic forces are approximated as rational functions by Minimum-State method, and the effect of compliant morphing trailing edge on the wing dynamic response is investigated. A Linear Quadratic Gaussian regulator is designed to explore the potential of suppressing wing flutter by deflecting the morphing trailing edges actively. Active suppression of aeroelastic response by controlling the trailing edge deflection validated through numerical simulations in the time domain. The simulation results show that the morphing trailing edges can increase the flutter boundary and change the flutter frequency.

Keywords: morphing, linear quadratic gaussian regulator, aeroservoelastic, high-aspect-ratio wing

1. Introduction

As the international awareness about the environmental protection is increasingly growing, the aircraft wing design tends to be a more and more lightweight, flexible, and high aspect design, to increase the aerodynamic efficiency and hence to reduce the emission by fuel-burn. However, such type of wing will increase the gust and maneuver loads and decrease the flutter margin, and furtherly affect the aircraft structural and aeroelastic stability. To cope with these problems, the concept of morphing trailing edge was proposed [1]. Up to now, the morphing trailing edges such as the Adaptive Compliant Trailing Edge (ACTE) by FlexSys [2] and the Variable Camber Continuous Trailing Edge Flap (VCCTEF) by Boeing and NASA [3] have been developed and tested.

The aeroservoelasticity is generally concerned with static aeroelastic trim, wing box structural tailoring, active flutter mitigation and gust alleviation using control surfaces. Many works have demonstrated the potential application of the morphing trailing edge to the flexible and high aspect wing [4–5]. Regarding the wing box design and optimization, Burdette conducted the aeroelastic optimization for a standard wing with morphing trailing edge, demonstrating that the morphing trailing edge can decrease the weight of wing box and hence can reduce the fuel burn [6]; Stanford designed a subsonic transport wing box under a variety of static and dynamic aeroelastic constraints, providing a quasi-steady deflection scheduling to a series of control surfaces that are distributed along the morphing trailing edge [7]. Nonetheless, these works did not consider the elastic and dynamic behavior of the compliant trailing edge. The ground test shows that the geometry changes have a significant effect on the frequencies [8]. To address this problem, De Gaspari et al. implemented a morphing trailing and managed to apply it to the Reference Aircraft [9]. Besides, to furtherly increase the performance gain, the distribute actuators has been widely implemented. Henry et al. performed a two-stage multidisciplinary design by optimizing the positions of piezoelectric actuators on the compliant structure, obtaining the rolling moment, and increasing the flutter speed without mass penalty [10].

In this paper, the following problems are to be addressed.

Aeroelastic modeling and analysis. The Double-Lattice Method (DLM) and rational functions approximation will be used to generate the unsteady aerodynamic forces and simulate the morphing

process in the time domain. Regarding the modeling of structure, instead of building up a full 3D finite element model, we will develop the morphing trailing edge system by ground vibration test to reduce the complexity of the problem. The flexibility of the morphing trailing edge devices will be considered.

Aeroservoelastic optimization. In the field of aeroservoelasticity, the open-loop control is widely used for maneuvers, such as rolling maneuver and elastic trim, whereas the closed-loop control is often used for gust load alleviation, flight control, and active flutter suppression. In this study, a flutter suppression system will be developed by closed-loop control to stabilize the aeroelastic plant.

Through this study, we are expecting to analyze the effect of the dynamic response of the morphing trailing edge and to design an optimal flutter suppression system that can enlarge the flutter boundary.

2. Reference Aircraft

The reference high-aspect-ratio aircraft model used in this study is shown in Figure 1. The aircraft adopts a double tailstock layout and has a straight wing with a span of 5.02 m. Additionally, the aircraft weights approximately 26.0 kg.

Figure 2 illustrates the elastic wing structure composed of a metal main spar and aerodynamic shape. Including the aerodynamic shape, the span of a single wing is 2.32 m with average aerodynamic chord length of 0.2168 m. Moreover, the chord lengths are 0.3 m at root and 1.2 m at the tip, and aspect ratio is 25.15, which belongs to a large aspect ratio aircraft. The main spar is manufactured by high-strength No. 7075 Aluminum alloy as the main load bearing component and weighs about 2.56 kg. The control surfaces are located at aft 40% chord length and 16% to 85% in the span direction. There are 6 actuated morphing trailing edges, each one can be controlled independently.

Figure 3 shows the finite element model of the reference aircraft. The structure dynamics characteristics of the wing are analyzed by MSC/NASTRAN software, and the results are listed below. First six modes (prime bending and torsion) are used in the modeling of Aeroservoelastic system. The elastic modal shapes of the first six orders for this aircraft are shown in Figure 4. It should be noted that the contribution of in-plane mode to flutter is negligible. Hence in-plane modes will be ignored in analysis.

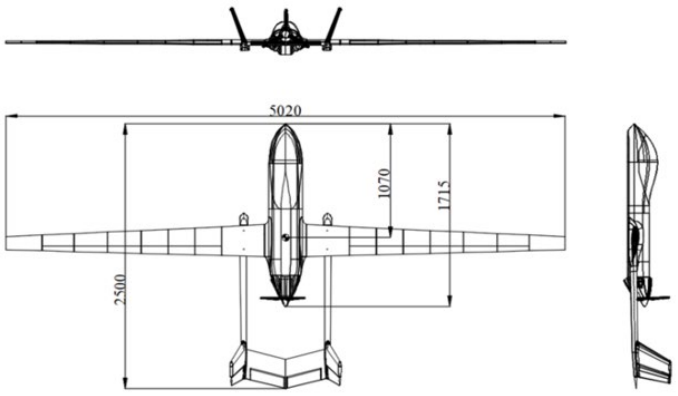

Figure 1 – Reference high-aspect-ratio unmanned aerial vehicle.

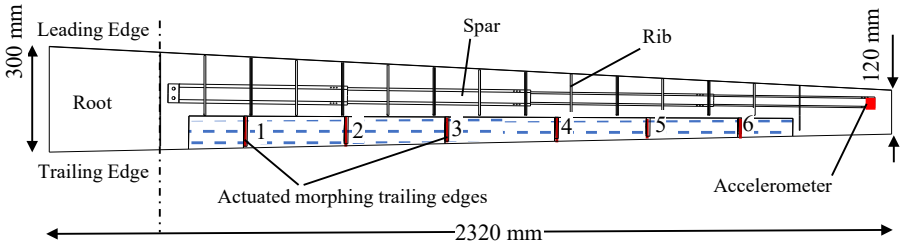

Figure 2 – High-aspect-ratio wing equipped with compliant morphing trailing edge.

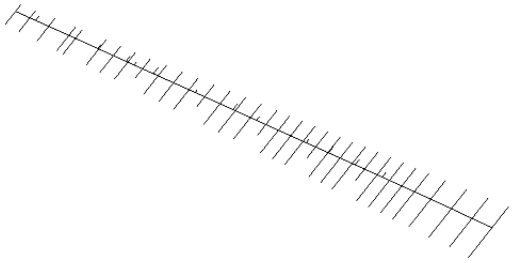

Figure 3 – Structural finite element model of wing.

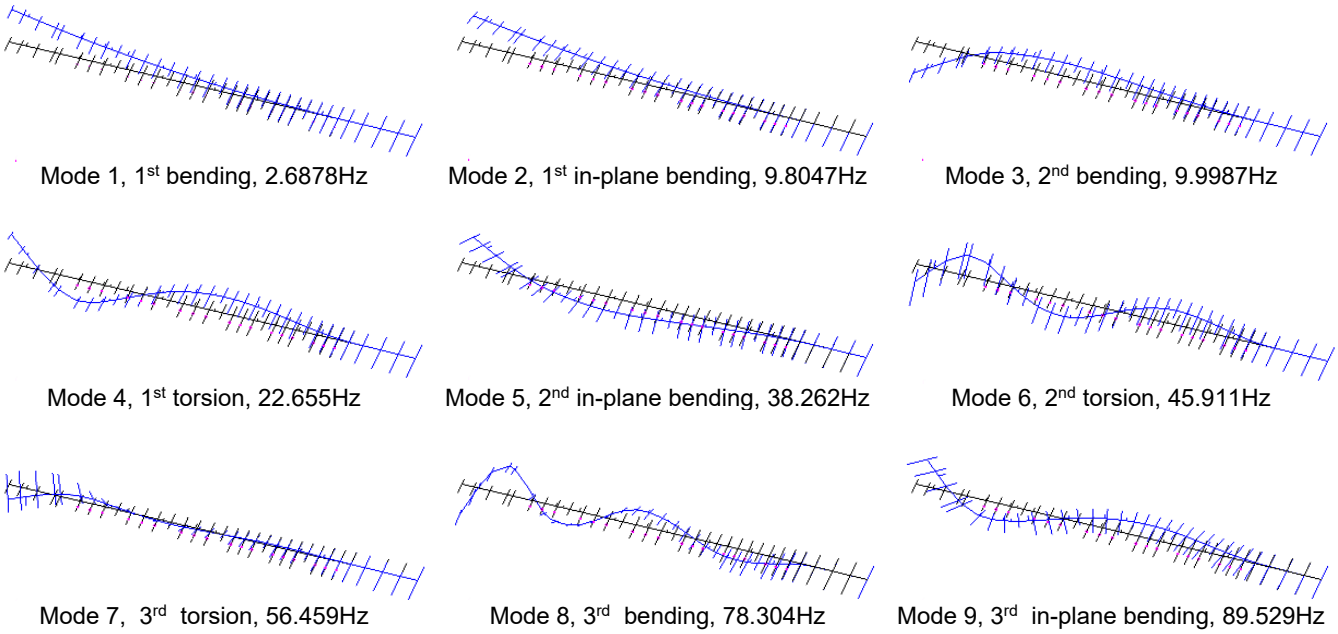

Figure 4 – Elastic modal shapes of the first 9 orders.

3. Methodologies

3.1 Modeling of Aerodynamic Grids for Unsteady Aerodynamic

Compared with the conventional control surface that rotated around the hinge axis, compliant morphing trailing edge deflects by elastic deformation. However, there is no center of rotation. In order to define the unit deformation of the compliant morphing trailing edge, it is assumed that the deformation beginning at the root of upper surface. Taking an airfoil as an example, literature [11] uses polynomials to describe different camber shapes of trailing edge, and presents an equivalent definition of unit deflection angle, reads:

$$\delta = \arctan\left(\frac{d_{\max}}{c_t}\right) \tag{1}$$

where, $d_{\max}$ is maximum vertical displacement of trailing edge, and c_t is the chord length of morphing part. For the unit deflection, $\delta_1 = 1°$. The camber shape of airfoil with morphing trailing edge described by polynomials can be expressed as:

$$\zeta_n(\psi) = \begin{cases} 0 & \psi \le \psi_{RS} \\ (\psi - \psi_{RS})^n \dfrac{\tan\delta_1}{(1-\psi_{RS})^{n-1}} & \psi_{RS} < \psi \le 1 \end{cases} \tag{2}$$

where, ψ is non-dimensional chord length, and ζ is the vertical position of the camber line. In this paper, second order polynomial shape is adopted, as shown in Figure 5.

Panel aerodynamic model (Double-Lattice Method) is used in this study, and the aerodynamic model is shown in Figure 6. The free stream velocity is fixed to 30 m/s at 0 km altitude

($\rho_{air} = 1.225\,kg/m^3$). Several aerodynamic force coefficient matrices at reduced frequencies ranging from 0.0 to 3.0 are calculated at Mach number of 0.45. The first unit deflection modes of compliant morphing trailing edges are shown in Figure 7. Please note that the vertical displacements have been zoom up 50 times for better illustration.

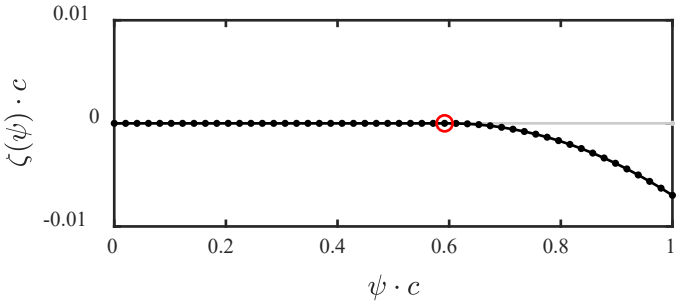

Figure 5 – Camber shape of morphing trailing edge, in which the red circle is assumed hinge.

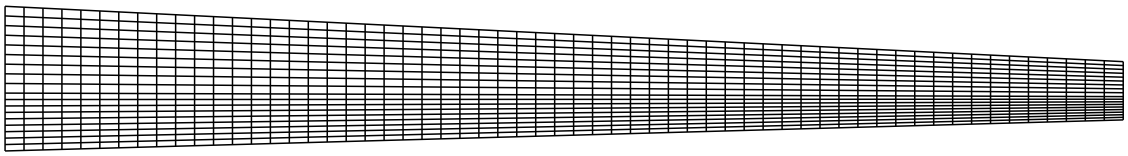

Figure 6 – Aerodynamic grid of wing component, 60 grids in span-wise and 20 in chord-wise.

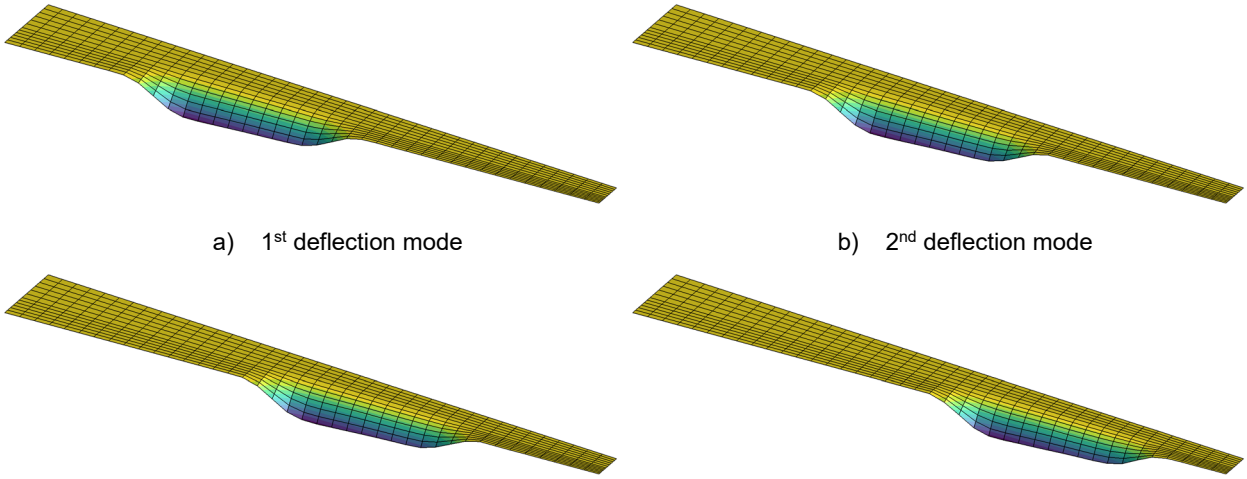

a) 1st deflection mode

b) 2nd deflection mode

c) 3rd deflection mode

d) 4th deflection mode

Figure 7 – Unit deflection modes of compliant morphing trailing edges.

3.2 Modeling of Aeroservoelastic System

The open-loop aero-servo-elastic equation is shown in Eq.(3)

$$\mathbf{M}_s\ddot{\boldsymbol{q}}_s + \mathbf{K}_s\boldsymbol{q}_s = \frac{1}{2}\rho V^2\left(\mathbf{Q}_s\boldsymbol{q}_s + \mathbf{Q}_c\mathbf{H}_c\boldsymbol{u}\right) \tag{3}$$

where, $\mathbf{M}_s$, $\mathbf{K}_s$ and $\mathbf{Q}$ are generalized mass matrix, stiffness matrix and aerodynamic matrix respectively, the subscript s represents structural elastic and c represents compliant morphing trailing edges. $\boldsymbol{q}_s$ is the generalized coordinates of structural elastic mode, ρ and V are air density and free-stream velocity, $\mathbf{H}_c$ is the transfer function from control input $\boldsymbol{u}$ to deflection angles $\boldsymbol{\delta}$.

The generalized aerodynamic matrix is a function of Mach number and reduced frequency and is approximated as rational function of the Laplace variables by means of Minimum-State method [12], and then coupled with structural dynamic system in time domain of both wing component and compliant morphing trailing edges. The number of lag states affect the fitting accuracy. In this paper, we use three lag states, and the approximating error is less than 0.2% [13].

The third-order transfer function is used to simulate the dynamic characteristics of the compliant morphing trailing edge system, including the structure flexibility and linear servo actuator. According to the results from ground vibration test, the bandwidth of morphing trailing edge is around 8 Hz [14]. The transfer function is shown in Eq.(4). Figure 8 demonstrates the open loop aeroservoelastic system of compliant morphing trailing edge wing.

$$\frac{\delta(s)}{u(s)} = \frac{9\times 2\pi}{s+9\times 2\pi}\cdot\frac{(7.7\times 2\pi)^2}{s^2+2\times 0.5\times 7.7\times 2\pi s+(7.7\times 2\pi)^2} \tag{4}$$

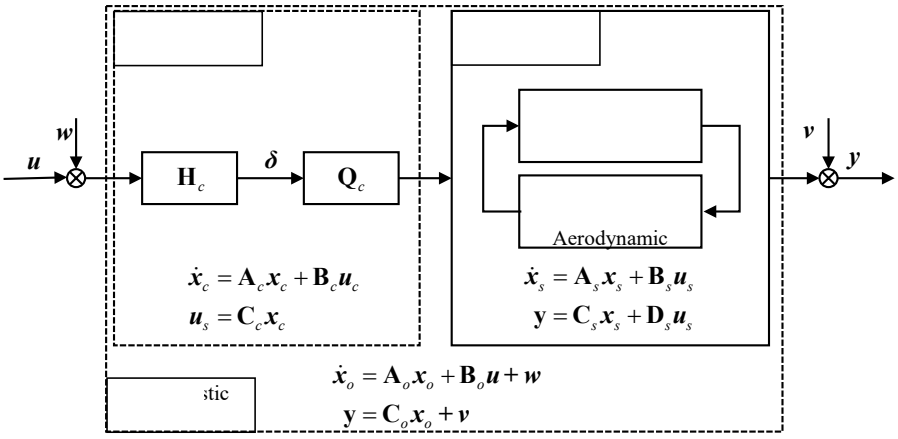

Figure 8 – Block diagram of open-loop aero-servo-elastic system.

3.3 Control Law

The deflection of morphing trailing edge may change the unsteady flow field around the wing, and thus affect the motion of the wing. The aeroelastic plant shown in Figure 9 contains the dynamics characteristics of morphing trailing edge with actuating system. When a proper controller is used, the morphing trailing edge will deflect to follow the command signal.

In aeroelastic, the aerodynamic states cannot be measured, so a full-state feedback controller is not available. Therefore, an observer is required for estimating the state-vector, based upon a measurement of the output. The linear-quadratic-Gaussian regulator (LQG) controller combines the optimal regulator and Kalman filter into an optimal controller, making it very suitable for active flutter suppression.

In order to design the infinite-horizon, continuous-time LQG controller, the performance index should be solved:

$$\min_{\boldsymbol{u}} J = E\left\{\lim_{\tau\to\infty}\frac{1}{\tau}\int_0^{\tau}\left(\boldsymbol{x}_o{}^T\mathbf{Q}\boldsymbol{x}_o + \boldsymbol{u}^T\mathbf{R}\boldsymbol{u}\right)dt\right\} \tag{5}$$

where $\mathbf{Q}$ and $\mathbf{R}$ are symmetric weighting matrix for states $\boldsymbol{x}_o$ and control inputs $\boldsymbol{u}$, $\mathbf{Q}$ is positive(semi) and $\mathbf{R}$ is positive definite.

Subject to the aeroelastic plant:

$$\begin{aligned}\dot{\boldsymbol{x}}_o &= \mathbf{A}_o\boldsymbol{x}_o + \mathbf{B}_o\boldsymbol{u} + \boldsymbol{w}\\ \mathbf{y} &= \mathbf{C}_o\boldsymbol{x}_o + \boldsymbol{v}\end{aligned} \tag{6}$$

where the process noise $\boldsymbol{w}$ and measurement noise $\boldsymbol{v}$ are assumed Gaussian white noises.

The construction of $\mathbf{Q}$ and $\mathbf{R}$ influences the performance of system. For example, $\mathbf{Q}$ provides the constraints of state response, and $\mathbf{R}$ bounds the control energy consumption. From the perspective of aeroelastic applications, it is essential for designer constructing appropriate weighting matrix $\mathbf{Q}$ and $\mathbf{R}$ to bound the control input of which the magnitude is generally less than 20 degrees. The whole block diagram of the closed loop system is shown in Figure 9. The stability of the closed loop system can also be analyzed by root-locus method.

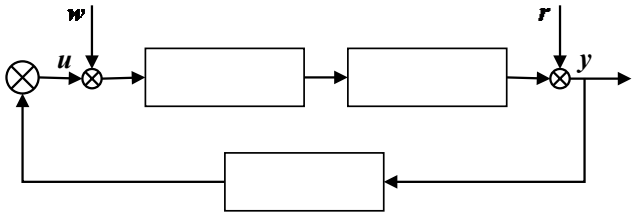

Figure 9 – Closed loop aeroelastic system with LQR controller.

4. Flutter characteristics of open-loop system

This section analyzes the flutter characteristics of the wing that does not use the morphing trailing edges by using the classic p-k method and eigenvalue of state space model.

The first 3 bending and torsional modes are selected for calculating the generalized aerodynamic force and for constructing the aeroelastic system. The first 3 in-plane bending modes are discarded because their influence on flutter characteristics are negligible. Previous studies have shown, using the above 6-order mode can capture the flutter characteristics with sufficient accuracy.

Use the classic p-k method to analyze the flutter characteristics of the system from frequency domain. The V-g and V-f diagrams are shown in Figure 10. The critical flutter velocity of the wing component is about $V_f = 148.6\text{m/s}$ with flutter frequency of 21.7Hz. It is mainly in the form of bending-torsional flutter coupled by modes 4 and 6, which manifests as the divergence of the fourth mode.

Figure 11 is the root-locus plot of the aeroelastic system in the form of state space for flutter prediction. When the airspeed is low, all eigenvalues are in the left-half plane, and the wing is stable. With the increasing airspeed, the eigenvalues of 4^{th} ,6^{th} and 7^{th} mode move rightwards, and the 4^{th} mode crosses the imaginary axis firstly. When the eigenvalue has crossed over into the right-half plane, the wing becomes unstable, and the critical flutter speed is $V_f = 148.5\text{m/s}$ and the corresponding flutter frequency is 21.5Hz, which are close to the results obtained by p-k method. This root-locus diagram indicates that the unsteady aerodynamics forces approximated by Minimum-State method and the subsequently state-space modeling are accurate.

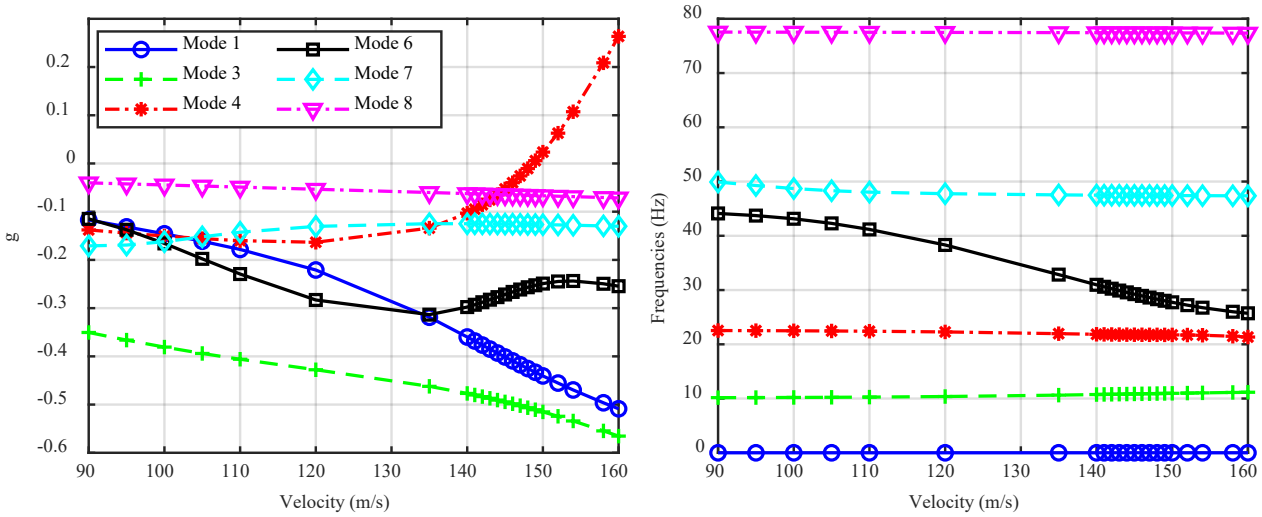

Figure 10 – V-g diagram for wing, flutter speed is about 148.5 m/s.

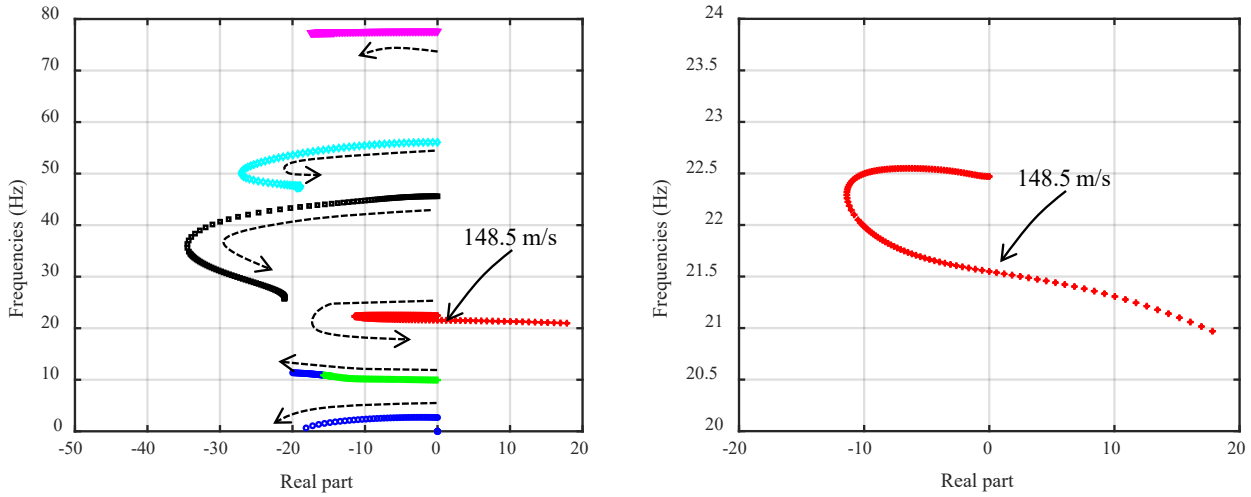

Figure 11 – Root locus of the open-loop state space system.

5. Active flutter suppression

The controller plays a key role in the closed-loop system because it can affect the wing flutter boundary and dynamic response. In this section, we firstly operate deflection modes 1-4 separately and investigate flutter suppression, and then operate deflection modes 1-4 simultaneously and investigate flutter suppression.

Without a controller, the critical flutter speed of the wing with compliant morphing trailing edge is $V_f = 148.5\text{m/s}$, as shown in Figure 10 and Figure 11. When the airspeed increases to $V^* = 150\text{m/s}$, the wing is unstable because the eigenvalues of 1st torsion mode has entered the right-half plane. Under this condition ($V = V^*$), the aeroelastic system is treated as a plant, then the LQG controller is designed.

In order to compare the effect of different deflection modes, the weighting matrices in LQG controller are set uniformly as $\mathbf{Q} = 10\mathbf{I}$ and $\mathbf{R} = 1\mathbf{I}$ for all deflection modes.

5.1 Flutter suppression through individual morphing trailing edge

The multiple-input multiple-output (MIMO) system with 4 inputs 1 output degenerates into a single-input single-output (SISO) when only one compliant morphing trailing edge is enabled. Based on this SISO system, the SISO LQG controller is designed, and the stability of the closed-loop system is investigated.

The root locus of closed-loop system for different compliant morphing trailing edges are plotted in the same speed range, as shown in Figure 12. Control modes appears in the root locus. And the critical flutter speeds for connecting different compliant morphing trailing edges are also shown in the plots. When using a single deflection mode, the introduction of deflection mode 2 can increase the flutter speed to $V_{u_2} = 155.5\,\text{m/s}$, with 4.7% increment. In addition, the flutter mode when the controller is present is consistent with the original wing.

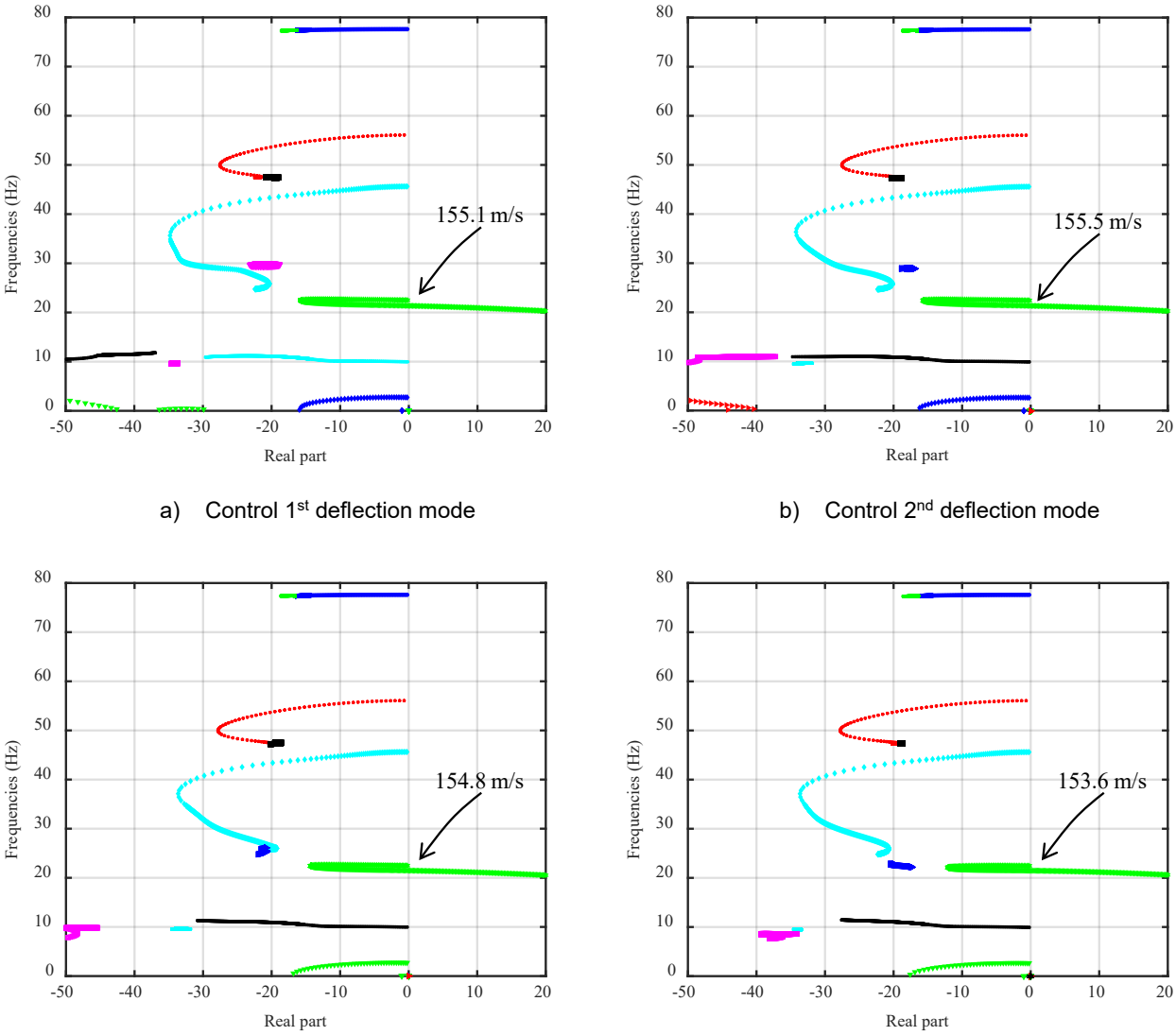

a) Control 1st deflection mode

b) Control 2nd deflection mode

c) Control 3rd deflection mode

d) Control 4th deflection mode

Figure 12 – Root-locus of closed-loop system with operating deflection modes 1-4 separately.

A comparison of the dynamic response for the systems applied disturbance reveals the effect of compliant morphing trailing edges on control efficiency. When the square wave pulse disturbance with an amplitude of 10 degrees and duration of applies on the 4th deflection mode at $t = 0\,\mathrm{s}$, the dynamic response of open-loop and closed-loop system is shown in Figure 13(a). After encountering a perturbation in the 4th deflection mode, the transient responses increase rapidly and tend to be diverging after several periods.

The controllers are enabled at $t = 1\,\mathrm{s}$, and Figure 13(b) demonstrates the control signal and true deflection. The blue dash-dot line is the LQG controller command output, and the red solid line is the true deflection of the trailing edge. With the active deflection of the trailing edges, the transient responses shown in Figure 13(a) at $t > 1\,\mathrm{s}$ decrease immediately and decay to almost zero with $1\,\mathrm{s}$. During the time history of each control mode deflection, the maximum angles of control command and true deflection are 4.22° and 1.2° at 4th deflection mode, respectively.

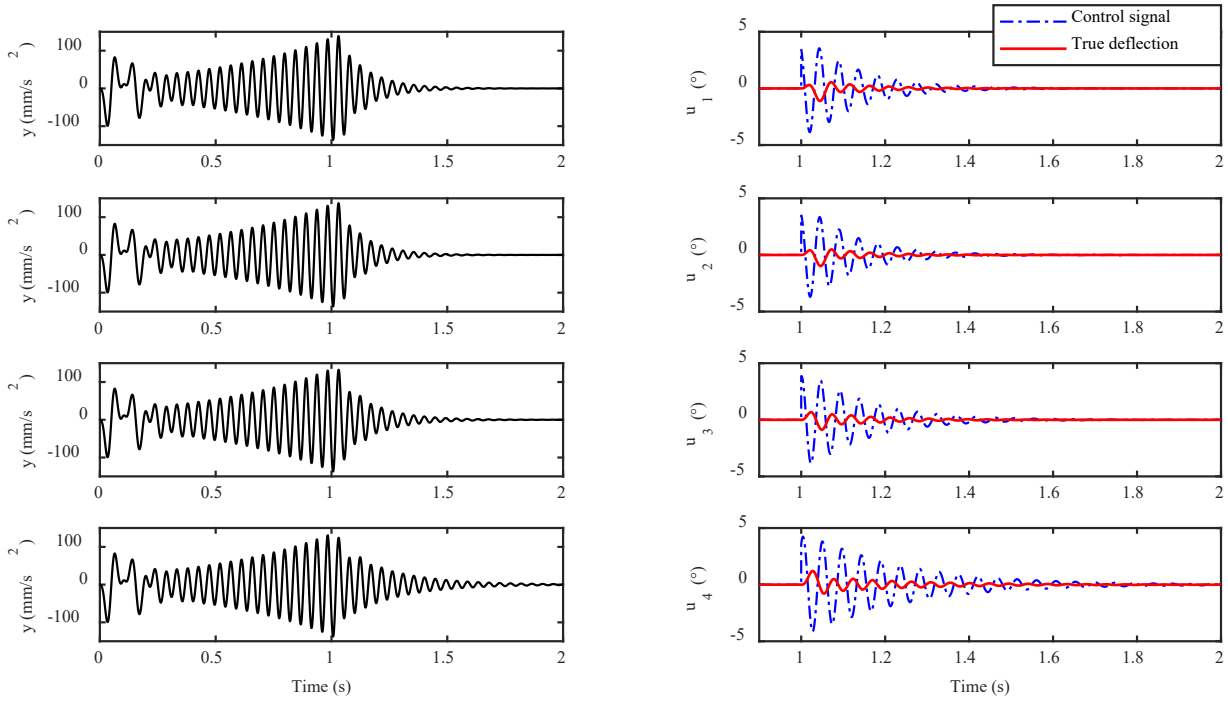

a) System output response

b) Control signals and deflections

Figure 13 – Open- and Closed-loop response with operating deflection modes 1-4 separately, at airspeed of 150 m/s.

5.2 Flutter suppression through full morphing trailing edge

This section presents the flutter suppression using all morphing trailing edge simultaneously. The root locus of open-loop system ($0<t<1\,\mathrm{s}$) and closed-loop system ($t>1\,\mathrm{s}$) are shown in Figure 14, including the structural modes and controller modes. The critical flutter speed is $158.5\,\mathrm{m/s}$, which is higher than the flutter speed obtained in previous section, and the increment is about 6.7%. The 2nd bending mode firstly moves left ward and then right, whereas the 2nd bending mode moves all the way to the left in Figure 12.

Figure 15 plots the transient response of open- and closed-loop system. The initial condition and perturbation are the same as the case in Figure 13. With the active deflection of the morphing trailing edge, the output response decreases immediately and decay to zero with $0.3\,\mathrm{s}$, which is faster than using single deflection mode. The maximum angles of control command are $+3.48^\circ$ and -2.88°, and the maximum angles of true deflection of morphing trailing edge are $+1.4^\circ$ and -1.1°.

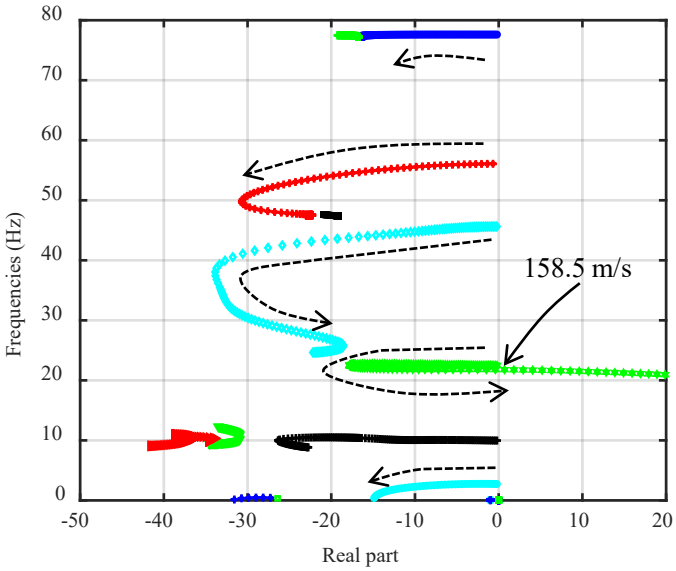

Figure 14 – Root-locus of closed-loop system with operating deflection modes 1-4 simultaneously.

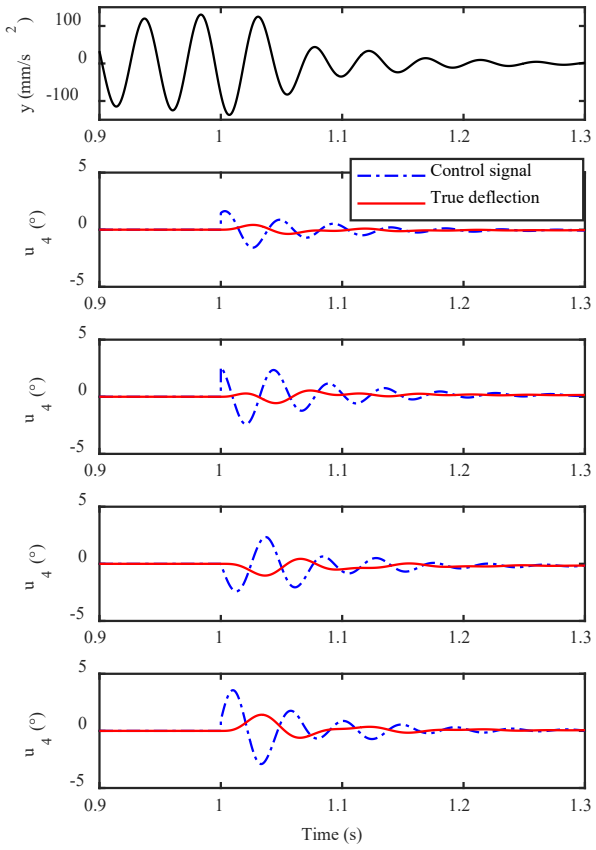

Figure 15 – Close-loop response with operating deflection modes 1-4 simultaneously.

6. Conclusion

1) The aero-servo-elastic modelling method of wing with compliant morphing trailing edges are presented using user-defined deflection modes.
2) Flutter speed can be increased to 155.5 m/s with increment of 4.71%, when using 2nd deflection mode.
3) With full span distribution of the morphing trailing edges, the flutter speed increases to 158.5 m/s with increment of 6.73%.
4) The efficient of flutter suspension is validated by time domain simulation.

7. Contact Author Email Address

Mail to: zk_zhang@buaa.edu.cn

8. Copyright Statement

References

[1] Scherer L B, Martin C A, West M N, et al. DARPA/ARFL/NASA Smart Wing Second Wind Tunnel Test R esults. *SPIE Conference on Industrial and Commercial Applications of Smart Structures,* Newport Beach , CA, United States, pp 249–259,1999.

[2] Kota S, Flick P, Collier F S. Flight Testing of FlexFloil TM Adaptive Compliant Trailing Edge. *54th AIAA A erospace Sciences Meeting.* Reston, Virginia, AIAA, pp 1–13, 2016.

[3] Ting E, Chaparro D, Nguyen N, et al. Optimization of Variable-Camber Continuous Trailing-Edge Flap C onfiguration for Drag Reduction. *Journal of Aircraft*, Vol. 55, No. 6, pp 2217–2239, 2019.

[4] Burdette D A, Kenway G K, Martins J. Performance Evaluation of a Morphing Trailing Edge Using Multip oint Aerostructural Design Optimization. *57th AIAA/ASCE/AHS/ASC Structures, Structural Dynamics, an d Materials Conference.* Reston, Virginia, AIAA, pp 1–15, 2016.

[5] Burdette D A, Martins J R R A. Impact of Morphing Trailing Edges on Mission Performance for the Com mon Research Model. *Journal of Aircraft*, Vol. 56, No. 1, pp 369–384, 2018.

[6] Burdette D A, Kenway G K, Lyu Z, et al. Aerostructural Design Optimization of an Adaptive Morphing Tra iling Edge Wing. *56th AIAA/ASCE/AHS/ASC Structures, Structural Dynamics, and Materials Conference.* Reston, Virginia, AIAA, pp 1–13, 2015.

[7] Stanford B K. Optimization of an Aeroservoelastic Wing with Distributed Multiple Control Surfaces. *Journ al of Aircraft*, Vol. 53, No. 4, pp 1131–1144, 2016.

[8] Herrera C, Spivey N, Lung S, et al. Aeroelastic Response of the ACTE Transition Section. *57th AIAA/AS CE/AHS/ASC Structures, Structural Dynamics, and Materials Conference.* Reston, Virginia, AIAA, pp 1–19, 2016.

[9] De Gaspari A, Ricci S, Travaglini L, et al. Active Camber Morphing Wings Based on Compliant Structure s: An Aeroelastic Assessment. *23rd AIAA/AHS Adaptive Structures Conference.* Reston, Virginia, AIAA, pp 1–13, 2015.

[10]Henry A C, Molinari G, Rivas-Padilla J R, et al. Smart Morphing Wing: Optimization of Distributed Piezoe lectric Actuation. *AIAA Journal*, Vol. 57, No. 6, pp 2384–2393, 2019.

[11]Forster E, Sanders B, Eastep F. Synthesis of a Variable Geometry Trailing Edge Control Surface. *44th A IAA/ASME/ASCE/AHS/ASC Structures, Structural Dynamics, and Materials Conference.* Reston, Virigina , AIAA, pp 2871–2882, 2003.

[12]Tiffany S, Karpel M. Aeroservoelastic Modeling and Applications Using Minimum-State Approximations o f the Unsteady Aerodynamics. *30th Structures, Structural Dynamics and Materials Conference*. Reston, Virigina, AIAA, pp 1–13, 1989.

[13]Song C, Yang C, Wu Z G. Comparison of three aeroelastic state-space modeling methods. *Acta Aerona utica et Astronautica Sinica*, Vol. 28 Sup., pp S81–S86, 2007 (in Chinese).

[14]Zhai H L. Drive Control Design and Quality Analysis of Flexible Rib on a Morphing Wing. *Beijing: Beihan g University*, pp 14–15, 2020 (in Chinese).